Supplemental material

Pion condensation in the early Universe at nonvanishing lepton flavor asymmetry and its gravitational wave signatures

Volodymyr Vovchenko,[1] Bastian B. Brandt,[2] Francesca Cuteri,[3]
Gergely Endrődi,[2] Fazlollah Hajkarim,[3] and Jürgen Schaffner-Bielich[3]

[1] *Nuclear Science Division, Lawrence Berkeley National Laboratory, 1 Cyclotron Road, Berkeley, CA 94720, USA*
[2] *Fakultät für Physik, Universität Bielefeld, D-33615 Bielefeld, Germany.*
[3] *Institut für Theoretische Physik, Goethe Universität Frankfurt, Max-von-Laue-Str. 1, D-60438 Frankfurt am Main, Germany*

I. EFFECTIVE MASS MODEL FOR PION CONDENSATION

We use a quasiparticle (effective mass) approach to describe interacting pions with a pion-condensed phase. Outside of the pion condensed phase, the pressure of a single pion species in the effective mass model reads [1]

$$p_\pi^{\rm EM}(T,\mu_\pi;m^*) = p_\pi^{\rm id}(T,\mu_\pi;m^*) + p_f(m^*). \qquad (1)$$

Here $\pi \in \pi^+,\pi^-,\pi^0$. The rearrangement term $p_f(m^*)$ is a consequence of interactions. It ensures a proper counting of the interaction energy and preserves the thermodynamic consistency in the quasiparticle model. For instance, it ensures that the quasiparticle pion number density, $n_\pi^{\rm EM} = n_\pi^{\rm id}(T,\mu_\pi;m^*)$, satisfies a thermodynamic relation $n_\pi^{\rm EM} = (\partial p_\pi^{\rm EM}/\partial\mu_\pi)_T$, correctly taking into account the medium dependence of the effective mass, $m^*(T,\mu)$. The specific form of $p_f(m^*)$ defines the quasiparticle model. Here we take $p_f(m^*)$ in the form

$$p_f(m^*) = \frac{(m^*)^2 f_\pi^2}{4}\left[1-\frac{m_\pi^2}{(m^*)^2}\right]^2, \qquad (2)$$

chosen to match the model to chiral perturbation theory and lattice QCD results in the pion-condensed phase at $T=0$ (see below). The pressure at a given T and μ_π has to be maximized with respect to m^*, resulting in a gap equation $(\partial p_\pi^{\rm EM}/\partial m^*)_{T,\mu}=0$:

$$p_f'(m^*) = n_\sigma^{\rm id}(T,\mu_\pi;m^*)\ . \qquad (3)$$

Here $n_\sigma^{\rm id}(T,\mu_\pi;m^*) \equiv -\partial p_\pi^{\rm id}/\partial m^*$ is the scalar density of an ideal gas of pions with mass m^*. A numerical solution to the gap equation determines m^* at given T and μ_π, allowing to calculate all other thermodynamic quantities through Eq. (2).

The transition to the pion-condensed phase takes place when the effective pion mass becomes equal to the chemical potential, $m^*=\mu_\pi$. The equation determining the transition line in the μ_π-T plane reads [1]

$$p_f'(\mu_\pi) = n_\sigma^{\rm id}(T,\mu_\pi;m^*=\mu_\pi)\ . \qquad (4)$$

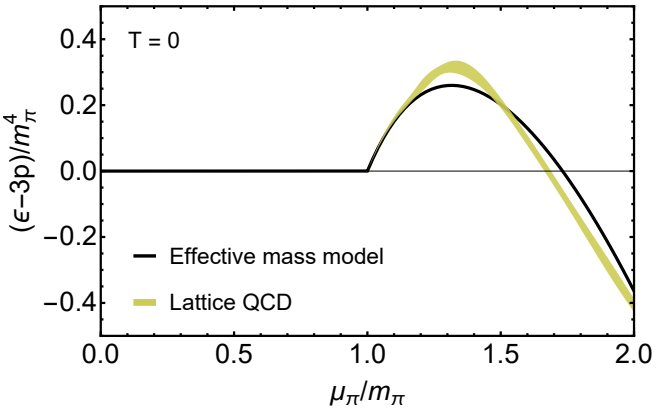

Figure 1. The dependence of the normalized trace anomaly $(\varepsilon-3p)/m_\pi^4$ on the normalized pion chemical potential μ_π/m_π, evaluated in the effective mass model at $T=0$. The yellow band depicts lattice QCD results from Ref. [2].

The effective mass equals the chemical potential in the phase diagram region with a pion condensate, $m^*=\mu_\pi$ for $\mu_\pi \geq \mu_{\rm cond}$, as a consequence of interactions between thermal and condensed pions [3]. Here $\mu_{\rm cond}$ is the pion chemical potential at pion condensation boundary. Therefore, the pressure in this phase reads reads

$$p_\pi^{\rm EM}(T,\mu_\pi) = p^{\rm id}(T,\mu_\pi;m^*=\mu_\pi) + p_f(\mu_\pi). \qquad (5)$$

At $T=0$, the pion number density $n_\pi^{\rm EM} = (\partial p_\pi^{\rm EM}/\partial\mu_\pi)_T$ reads

$$\begin{aligned} n_\pi^{\rm EM}(T=0,\mu_\pi) &= p_f'(\mu)\,\theta(\mu-m_\pi) \\ &= \frac{\mu_\pi f_\pi^2}{2}\left[1-\frac{m_\pi^4}{\mu_\pi^4}\right]\theta(\mu-m_\pi). \end{aligned} \qquad (6)$$

Equation (6) matches the result of leading-order chiral perturbation theory [4], which for $f_\pi = 133$ MeV describes well the available lattice QCD data on isospin density at $T=0$ [2]. Recently, these chiral perturbation theory predictions have been backed up by next-to-leading-order calculations, both for the density and for the equation of state [5–8].

II. LATTICE SIMULATIONS

Here we describe the details of our first-principles lattice QCD simulations at nonzero isospin density. On the one hand, the lattice results at (approximately) zero temperature are used to guide the construction of the effective mass model described above. Here we use our data at a single lattice spacing from Ref. [2]. On the other hand, the finite-temperature results serve to test the validity range of the model at nonzero isospin and zero baryon density. To this end we employ our data from Refs. [9, 10] on four lattice spacings.

To simulate the path integral $\mathcal{Z}$ we take the tree-level Symanzik-improved gauge action and $2+1$ flavors of rooted staggered quarks with physical masses [11]. The isospin chemical potential μ_I enters the Dirac operator[1] via the quark chemical potentials $\mu_u = -\mu_d = \mu_I/2$, while $\mu_s = 0$. Comparing to the standard basis with baryon and charge chemical potentials, one can read off $\mu_Q = \mu_I$, $\mu_B = -\mu_I/2$. The simulations therefore correspond to a situation with a specific linear combination of baryon and charge chemical potentials, which only couples to hadron species containing an unequal number of up and down quarks (predominantly charged pions).[2] To be able to perform the simulations, we further need to introduce an auxiliary pionic source $\lambda > 0$ that is extrapolated to zero at the end of the analysis. The role of the λ parameter is twofold. First, it triggers the spontaneous symmetry breaking corresponding to pion condensation in a finite volume. Second, it serves to stabilize the theory in the infrared by making the Goldstone boson of the pion condensed phase slightly massive [9].

To calculate the equation of state, our primary observable is the isospin density

$$n_I(T,\mu_I) = \frac{T}{V}\frac{\partial \log \mathcal{Z}}{\partial \mu_I}\,. \tag{7}$$

The details of the $\lambda \to 0$ extrapolation of this observable are explained in Ref. [10] and in the following we work with the so extrapolated quantity. From n_I, we can calculate $\Delta\mathcal{O}(T,\mu_I) \equiv \mathcal{O}(T,\mu_I) - \mathcal{O}(T,0)$ for any observable $\mathcal{O}$. In particular, the pressure difference and the trace anomaly difference can be constructed as

$$\Delta p(T,\mu_I) = \int_0^{\mu_I} \mathrm{d}\mu_I'\, n_I(T,\mu_I')\,, \tag{8}$$

$$\Delta I(T,\mu_I) = \mu_I n_I(T,\mu_I) + \int_0^{\mu_I} \mathrm{d}\mu_I' \left(T\frac{\partial}{\partial T} - 4\right) n_I(T,\mu_I')\,. \tag{9}$$

The zero-temperature results for n_I near $\mu_I = m_\pi$ are well-described by the chiral perturbation theory formula (6) with $f_\pi = 133(4)$ MeV [2, 5–8]. This is smoothly matched by a spline interpolation for $n_I(\mu_I)$ at higher values of the chemical potential. The interaction measure is determined via Eq. (9) – note that at zero temperature $\Delta I = I$ and, moreover, the first contribution to the integral in ΔI of Eq. (9) vanishes, simplifying this expression considerably. The so obtained curve is plotted in Fig. 1 as the yellow band.

For testing the effective mass model at $T > 0$ we concentrate on ΔI because compared to other observables

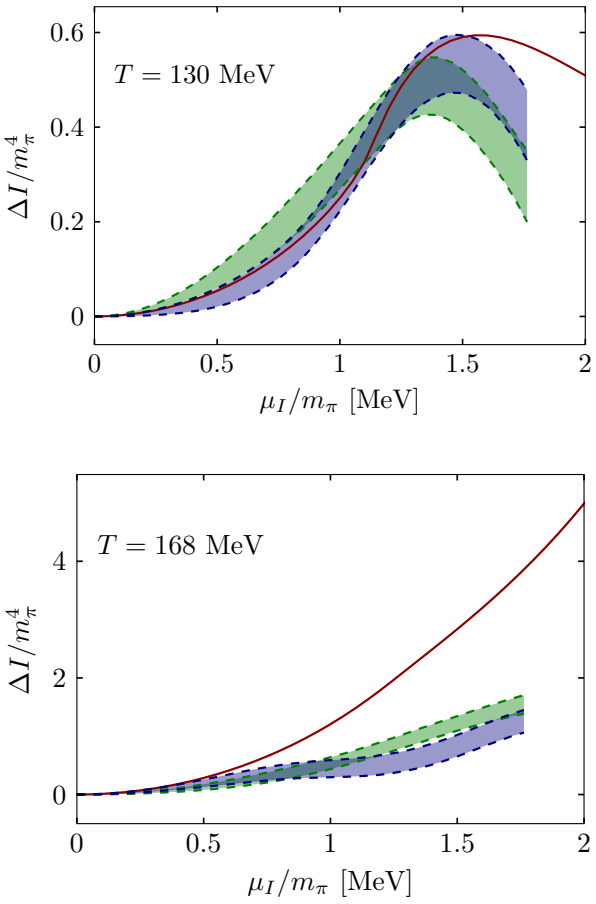

Figure 2. The trace anomaly difference as a function of μ_I at two different temperatures on our $N_t = 10$ (green) and $N_t = 12$ (blue) lattice ensembles, compared to the effective mass model (red curve).

[1] This convention, for which pion condensation sets in at $\mu_I = m_\pi$ at zero temperature, differs from that used in our earlier works [9, 10] by a factor of two.

[2] Note that the baryon density still vanishes in our simulations: it is obtained in terms of derivatives with respect to the quark chemical potentials as $n_B = n_u/3 + n_d/3 + n_s/3 = 0$ at pure isospin chemical potential, where $n_u = -n_d$ and $n_s = 0$.

it is found to contain the least amount of lattice discretization errors[3]. The integrals and the derivatives in Eq. (9) need to be evaluated numerically. To this end we fit $n_I(T, \mu_I)$ via a two-dimensional spline surface. The spline nodepoints are drawn from a Monte-Carlo procedure with the goodness of the fit playing the role of the action, providing a direct estimate of systematic errors (see Ref. [12] for more details). The μ_I-dependence of ΔI is plotted for two representative values of the temperature in Fig. 2. Here we include the results for our two finest lattice spacings, $N_t = 10$ and $N_t = 12$. (The continuum limit at constant T corresponds to $N_t \to \infty$, but we do not carry out this extrapolation here.) The model is found to capture the notable features of the lattice data qualitatively. A quantitative description is obtained if neither T nor μ_I are too large. In particular, sizeable deviations are visible above the chiral restoration temperature, because the effective mass model does not contain the details of the physics of this phase transition.

To make the comparison between the $N_t = 12$ lattice results and the model more systematic, in Fig. 3 we show the deviation between the two in the form of a heat plot. Here we normalize by the error σ of the lattice results – therefore a value of n indicates a difference by n standard deviations. The plot shows substantial differences for $\mu_I > m_\pi$ at high temperatures as well as slight deviations near the boundary of the pion condensed phase. We take the contour line at 3 standard deviations as a marker and consider the model reliable in the parameter range where

$$\frac{|\Delta I - \Delta I^{\mathrm{EM}}|}{\sigma(\Delta I)} \leq 3\,, \tag{10}$$

with ΔI^{EM} being the subtracted interaction measure in the effective mass model. This range is indicated by the solid line sections of the cosmic trajectories in Fig. 1 of the main text.

The above comparisons were performed at nonzero isospin chemical potential μ_I, where lattice results are available. For the analysis of the cosmic trajectory, the model is employed instead at nonzero charge chemical potential μ_Q (as well as low baryon chemical potential μ_B). At zero temperature, μ_I and μ_Q can be identified as long as the only charged states that contribute to the equation of state have zero strangeness and zero baryon number. This is the case for $\mu_I < m_K$ (even in this case, kaon condensation is not expected to occur if a pion condensate is already present [13]) and sufficiently low μ_B as is the case for the parameters considered in this paper.

[3] Note that this choice allows to discuss the μ_I-dependence of the model but not its reliablility at $\mu_I = 0$. However, for the effect of pion condensation on the cosmic trajectory, we expect the latter to be less important.

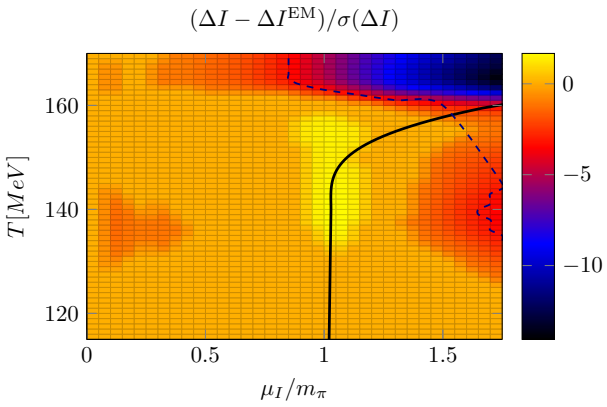

Figure 3. Heat plot of the deviation between the effective mass model and the lattice results for the trace anomaly difference ΔI. For the latter our finest, $N_t = 12$ ensembles are used. The deviation is normalized by the error of the lattice data. The solid black line indicates the lattice result for the pion condensation boundary, while the dashed line denotes the contour of 3.

Contrary to the identification $\mu_I = \mu_Q$ at zero temperature, for $T > 0$ the different couplings of the two chemical potentials to hadronic states becomes relevant and the equation of state differs in the two cases. Nevertheless, in the effective mass model the pion condensation boundary expressed in μ_I or in μ_Q remains the same, because interactions between pions and other hadrons are neglected in the model. The difference between the critical lines, $\mu_Q^{\mathrm{crit}}(T)$ and $\mu_I^{\mathrm{crit}}(T)$ can be estimated using lattice results for the estimators of the convergence radii of the corresponding Taylor series around $\mu_Q = \mu_I = 0$. In particular, we consider the expansions of the pressure,

$$\frac{p}{T^4} = \frac{c_2^{I,Q}}{2}\left(\frac{\mu_{I,Q}}{T}\right)^2 + \frac{c_4^{I,Q}}{24}\left(\frac{\mu_{I,Q}}{T}\right)^4 + \dots \tag{11}$$

and the estimators for the convergence radius for the susceptibilities $\chi_{I,Q} = \partial^2 p/\partial \mu_{I,Q}^2$. We use the Taylor coefficients determined in Ref. [14] for our action and lattice spacings. The leading estimator

$$\frac{r_2(\chi_{I,Q})}{T} = \sqrt{\frac{2c_2^{I,Q}}{c_4^{I,Q}}}\,, \tag{12}$$

for the isospin direction was found to give a remarkably good approximation to the true critical line, μ_I^{crit} [10]. We assume this is also the case for the expansion in μ_Q. Thus we approximate the critical line in the electric charge direction by

$$\mu_Q^{\mathrm{crit}} \approx \mu_I^{\mathrm{crit}} \cdot \frac{r_2(\chi_Q)}{r_2(\chi_I)}\,. \tag{13}$$

For the second factor we use the lattice results [14] above and ideal HRG with quantum statistics below a matching

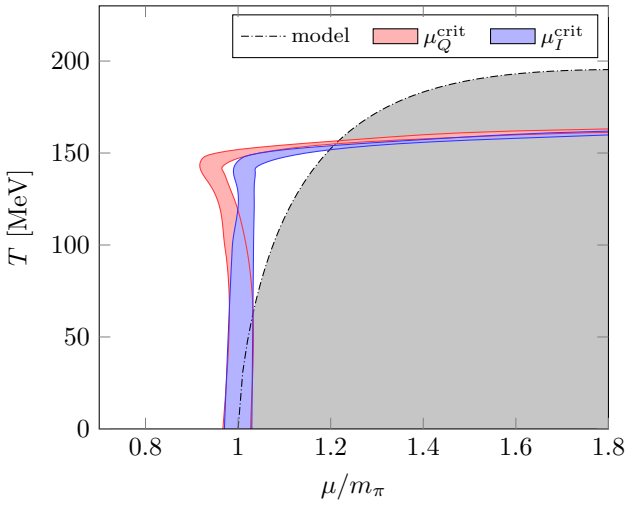

Figure 4. The critical lines $\mu_Q^{\rm crit}$ and $\mu_I^{\rm crit}$ as obtained on $N_t = 12$ lattices from the approximation in Eq. (13) and from direct simulations, respectively. The critical line from the effective mass model is included for comparison.

temperature of 105 MeV. The $N_t = 12$ results for this approximation, together with the corresponding directly determined isospin critical line $\mu_I^{\rm crit}$ [9, 10], are plotted in Fig. 4.

Comparing to the effective mass model, quantitative differences are observed for $T \gtrsim 80$ MeV. While this bound is comparable to recent results in chiral perturbation theory to next-to-leading order [8], where the agreement persists up to about $T \gtrsim 40$ MeV, other models, such as the Nambu-Jona-Lasinio [15] or the Polyakov loop-extended quark meson model [16, 17], for instance, show better agreement, both qualitatively and quantitatively, with the lattice phase diagram (see also Fig. 9 of Ref. [13]). In particular, both models reproduce the steep rise in combination with the leveling-off of the BEC phase boundary at large μ_I. Nonetheless, the qualitative agreement between the effective mass model and the lattice data together with the fact that the lattice results for $\mu_I^{\rm crit}$ and $\mu_Q^{\rm crit}$ do not differ by more than a few percents again confirms that our model represents a reasonable approximation to the phase diagram at nonzero isospin (charge) densities. In addition, the inclusion of further hadrons and resonances in the effective mass model is straightforward.

III. PRIMORDIAL BLACK HOLES FORMATION

At the time of PBH formation a region of the Universe within the Hubble horizon starts to collapse due to local

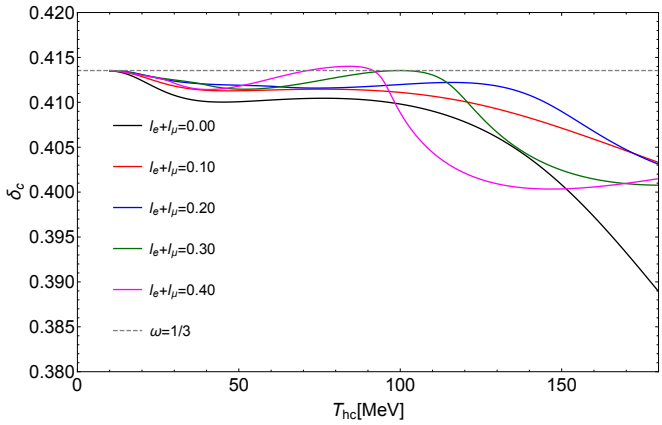

Figure 5. Threshold of primordial black hole formation versus horizon crossing temperature for different values of the lepton asymmetry.

inhomogeneities amounting to

$$\beta(M) = \frac{M_{eq}}{M}\beta_{eq}\,. \tag{14}$$

The relation between the amplitude of the density perturbation δ, the PBH mass $M_{\rm BH}$ and the horizon mass M_h can be defined as [18, 19]

$$\delta = \left(\frac{M_{\rm BH}}{KM_h}\right)^{\frac{1}{\gamma}} + \delta_c\,. \tag{15}$$

The parameters in Eq. (15) are obtained from numerical simulations to be $K = 3.3$ and $\gamma = 0.36$ [18–23]. The parameter δ_c is the threshold for PBH formation where different estimates for it exist in the literature [18, 19, 22–26]. Here we assume that this threshold in a cosmological background slightly deviates from the one of a purely radiation dominated Universe ($\omega = p/\varepsilon = 1/3$) which is estimated to be $\delta_c \simeq 0.41$ [25, 26]. Variation of δ_c due to different lepton asymmetry values is shown in Fig. 5.

The fraction of PBHs $\Omega_{\rm PBH}$ with respect to the total cold dark matter (CDM) abundance $\Omega_{\rm CDM}$ reads [27]

$$f_{\rm PBH}(M_{\rm BH}) = \frac{1}{\Omega_{\rm CDM}}\int_0^\infty \frac{2dM_h}{\sqrt{2\pi\sigma(M_h)^2}}\frac{M_{\rm BH}}{\gamma M_h}\times \exp\left[-\frac{\delta^2(M_h)}{2\sigma^2(M_h)}\right]\left(\frac{M_{\rm BH}}{KM_h}\right)^{\frac{1}{\gamma}}\sqrt{\frac{M_{eq}}{M_h}}\,. \tag{16}$$

The mass or scale dependence of the density perturbation width can be assumed to be [27]

$$\sigma^2(M_h) = 0.003\left(\frac{M_h}{10M_\odot}\right)^{n_M}\,. \tag{17}$$

The density spectral index n_M can be related to the scalar spectral index $n_S - 1 \simeq -2n_M$, where $n_S \simeq 0.96$ [28, 29]. We choose the benchmark value of $n_M = 0$ to

compute the fraction of PBH from Eq. (16). The parameter $f_{\rm PBH}$ for masses smaller than $M_\odot$ increases (decreases) when n_M is negative (positive). However, $f_{\rm PBH}$ increases (decreases) for larger masses, respectively. For a fixed n_M as lepton asymmetry increases the value of $f_{\rm PBH}$ will change depending on the behavior of ω or δ_c and the energy and pressure density. When δ_c increases (decreases) the fraction of PBH decreases (increases).

[1] O. Savchuk, Y. Bondar, O. Stashko, R. V. Poberezhnyuk, V. Vovchenko, M. I. Gorenstein, and H. Stoecker, Phys. Rev. C **102**, 035202 (2020), arXiv:2004.09004 [hep-ph].

[2] B. B. Brandt, G. Endrődi, E. S. Fraga, M. Hippert, J. Schaffner-Bielich, and S. Schmalzbauer, Phys. Rev. D **98**, 094510 (2018), arXiv:1802.06685 [hep-ph].

[3] H. Barz, B. Friman, J. Knoll, and H. Schulz, Phys. Rev. D **40**, 157 (1989).

[4] D. Son and M. A. Stephanov, Phys. Rev. Lett. **86**, 592 (2001), arXiv:hep-ph/0005225.

[5] P. Adhikari and J. O. Andersen, Phys. Lett. B **804**, 135352 (2020), arXiv:1909.01131 [hep-ph].

[6] P. Adhikari and J. O. Andersen, JHEP **06**, 170 (2020), arXiv:1909.10575 [hep-ph].

[7] P. Adhikari and J. O. Andersen, (2020), arXiv:2003.12567 [hep-ph].

[8] P. Adhikari, J. O. Andersen, and M. A. Mojahed, (2020), arXiv:2010.13655 [hep-ph].

[9] B. Brandt, G. Endrődi, and S. Schmalzbauer, Phys. Rev. D **97**, 054514 (2018), arXiv:1712.08190 [hep-lat].

[10] B. B. Brandt and G. Endrődi, Phys. Rev. D **99**, 014518 (2019), arXiv:1810.11045 [hep-lat].

[11] S. Borsányi, G. Endrődi, Z. Fodor, A. Jakovác, S. D. Katz, S. Krieg, C. Ratti, and K. K. Szabó, JHEP **11**, 077 (2010), arXiv:1007.2580 [hep-lat].

[12] B. B. Brandt and G. Endrődi, PoS **LATTICE2016**, 039 (2016), arXiv:1611.06758 [hep-lat].

[13] M. Mannarelli, Particles **2**, 411 (2019), arXiv:1908.02042 [hep-ph].

[14] S. Borsányi, Z. Fodor, S. D. Katz, S. Krieg, C. Ratti, and K. Szabó, JHEP **01**, 138 (2012), arXiv:1112.4416 [hep-lat].

[15] L.-y. He, M. Jin, and P.-f. Zhuang, Phys. Rev. D **71**, 116001 (2005), arXiv:hep-ph/0503272.

[16] P. Adhikari, J. O. Andersen, and P. Kneschke, Phys. Rev. D **98**, 074016 (2018), arXiv:1805.08599 [hep-ph].

[17] A. Folkestad and J. O. Andersen, Phys. Rev. D **99**, 054006 (2019), arXiv:1810.10573 [hep-ph].

[18] J. C. Niemeyer and K. Jedamzik, Phys. Rev. Lett. **80**, 5481 (1998), arXiv:astro-ph/9709072.

[19] J. C. Niemeyer and K. Jedamzik, Phys. Rev. D **59**, 124013 (1999), arXiv:astro-ph/9901292.

[20] C. R. Evans and J. S. Coleman, Phys. Rev. Lett. **72**, 1782 (1994), arXiv:gr-qc/9402041.

[21] T. Koike, T. Hara, and S. Adachi, Phys. Rev. Lett. **74**, 5170 (1995), arXiv:gr-qc/9503007.

[22] I. Musco, J. C. Miller, and A. G. Polnarev, Class. Quant. Grav. **26**, 235001 (2009), arXiv:0811.1452 [gr-qc].

[23] I. Musco, J. C. Miller, and L. Rezzolla, Class. Quant. Grav. **22**, 1405 (2005), arXiv:gr-qc/0412063.

[24] K. Jedamzik, Phys. Rev. D **55**, 5871 (1997), arXiv:astro-ph/9605152.

[25] T. Harada, C.-M. Yoo, and K. Kohri, Phys. Rev. D **88**, 084051 (2013), [Erratum: Phys.Rev.D 89, 029903 (2014)], arXiv:1309.4201 [astro-ph.CO].

[26] A. Escrivà, C. Germani, and R. K. Sheth, Phys. Rev. D **101**, 044022 (2020), arXiv:1907.13311 [gr-qc].

[27] C. T. Byrnes, M. Hindmarsh, S. Young, and M. R. S. Hawkins, JCAP **08**, 041 (2018), arXiv:1801.06138 [astro-ph.CO].

[28] Y. Akrami *et al.* (Planck), (2018), arXiv:1807.06211 [astro-ph.CO].

[29] N. Aghanim *et al.* (Planck), (2018), arXiv:1807.06209 [astro-ph.CO].